JOURNAL OF PROPULSION AND POWER
Vol. 20, No. 3, May–June 2004

Thrust-Vector Characteristics of Jet Vanes Arranged in X-Formation Within a Shroud

Hong-Gye Sung* and Yong-Seok Hwang†
Agency for Defense Development, Daejeon 305-600, Republic of Korea

Thrust-vector characteristics of jet vanes arranged in an X formation within a thrust-vector-control (TVC) shroud are very unique and much more complicated than those of the jet vanes acting without the shroud because of both the flow interference between the vanes and the shroud and the X formation of the vanes. The fluid dynamic interferences, such as the impingement of shock waves induced by jet vanes on the shroud wall, and the aerodynamic performance of jet vanes arranged in an X formation were investigated to characterize thrust vector control of jet vanes operating within the TVC shroud. An integrated method consisting of a semi-empirical model, a three-dimensional numerical analysis, and static firing tests of full-scale motors was applied to quantitatively present the side-force coefficient. Satisfactory agreement is found when compared to static firing test results.

Nomenclature

A	=	area
C	=	coefficient
l	=	distance between the leading edge of vane and nozzle exit
M	=	Mach number
P	=	static pressure
q	=	dynamic pressure
r	=	radius
α	=	deflection angle of vane
β	=	direction angle of the force on a shroud
γ	=	specific heat ratio
η	=	aerodynamic correction factor
κ	=	coefficient for identification of vane position
ξ	=	correction factor

Subscripts

av	=	averaged value
b	=	vane base
e	=	nozzle exit
i	=	index of vane
L	=	lift force
N	=	normal direction
p	=	vertical direction on shroud wall
s	=	shroud
t	=	throat of nozzle
v	=	vane
y	=	horizontal direction on shroud wall
1,2,3,4	=	identification number of vanes

Superscript

∞	=	freestream condition

I. Introduction

THE vehicle using aerodynamic control surfaces has poor high-alpha pitch-over characteristics in the launching stage because the missile speed just after launch is not fast enough to provide sufficient aerodynamic force to pitch over quickly. Thus, the use of the aerodynamic controls results in very high apogees before the missile can aerodynamically pitch over toward the target.[1] The thrust-vector-control (TVC) system was developed as an alternative in order to resolve the slow pitch-over of the aerodynamic control system. The TVC system can allow the missile to turn quickly and stably in any direction by deflecting the direction of the nozzle exhaust gas. Figure 1 identifies the relative gain achievable by vertical launch systems with the jet-vane TVC over conventional aerodynamic controls. (The trajectories shown in Fig. 1 represent fly-outs to the same target.[1]) The TVC system can be achieved with secondary injection of gas into the nozzle gas flow, the movable nozzle, the jet vanes, the jet tabs, and many others.[2–4] In case of tactical missile systems, jet vanes, jetavator, and jet tabs are widely used because they can be designed and manufactured to be relatively simple and compact.[3] Among them, the jet-vane TVC system is the most widely used because roll control is possible as well as the control of pitch and yaw.[5,6]

The basic principal of providing control forces using vanes is the same as that of getting lift using a supersonic wing at an angle of attack to the freestream. As a vane is deflected at a typical angle to exhaust gas, an oblique shock produced on a windward side of the vane introduces surface-pressure increases, whereas expansion waves produced on a leeward side of the vane cause surface pressure to decrease. The pressure difference between the windward and leeward sides of the vane provides a force normal to the chord of the vane. The normal force comes to be divided into two components: 1) lift, called side force, useful to control of the missile and 2) drag, resulting in thrust loss. The smaller the ratio of thrust loss to side force is, the better the performance of the vane is. To achieve high performance of the vane, a double-wedge type with some aspect ratio is widely used. However, the small round edge of the vane is employed instead of the sharp edge to preserve the initial shape of the vane from thermal ablation induced by hot exhaust gas passing through a nozzle.

The general shape of vanes is similar to that of supersonic wings. They both, for example, have a double wedge with some aspect ratio. Therefore, theoretical analysis,[7] experiment,[8] and numerical research[9] of a supersonic wing can help us to understand the characteristics of the single vane. In addition to studies on aerodynamic supersonic wings, some other previous research is useful to understanding the basic physical phenomena around vanes. The history of jet vanes and their basic design principals has been described by Ripley-Lotee and O'Neil.[10] Roger and his colleagues numerically studied the flowfields in the vicinity of a jet vane mounted at the exit of a nozzle using upwind flux difference splitting Navier–Stokes (UFDSNS) Navier–Stokes code.[11] The aerodynamic performance of single and four vanes was investigated by Euler solver.[12] Danielson and his colleagues pointed out that the aluminum oxide of combustion gas degrades the vane performance as a result of the

Received 5 December 2002; revision received 23 May 2003; accepted for publication 17 July 2003.

*Research Engineer, Tech-4-2; hgsung1@hananet.net.
†Research Engineer, Tech-4-2.

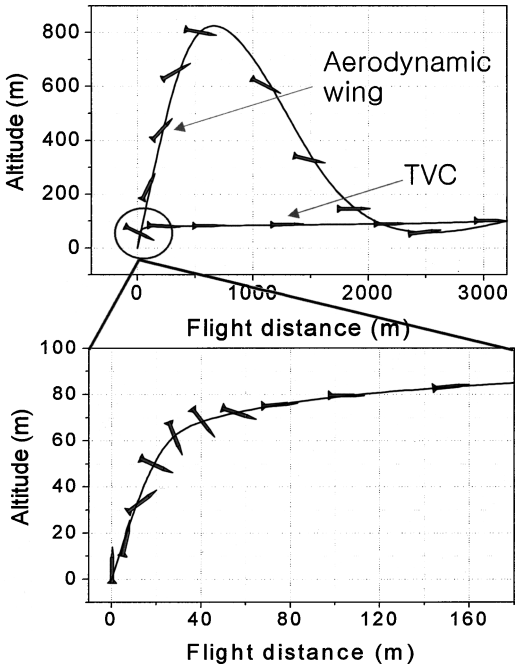

Fig. 1 Comparison of pitch-over between jet vane TVC and aerocontrol.[1]

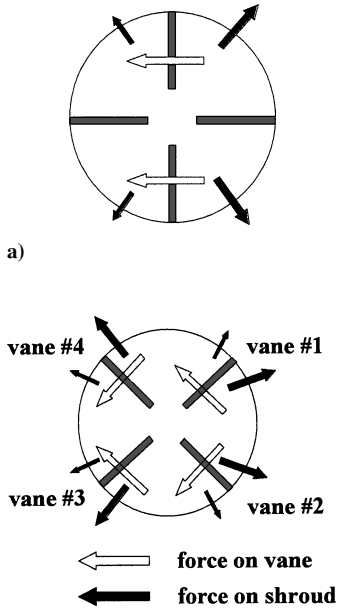

Fig. 2 Schematics and photo of jet vanes within the TVC shroud. a) + formation of vanes b) X formation of vanes c) prototype of X formation vanes within a shroud.

ablation of the leading edge of the vane.[1,13] However, all of the preceding research papers are related to jet vanes operating without a shroud, but not to jet vanes acting within the TVC shroud, which is subject of this paper. The jet-vane TVC system considered in this paper is unique in that four vanes with an X formation are surrounded by a conical shroud (see Fig. 2). Very limited information regarding vanes acting within a shroud is available in the literature.

Figure 2 shows the conceptual schematics of force vectors acting on both the vanes and the shroud. As shown, the TVC shroud generates additional forces, which are closely related to the flow patterns surrounding the four vanes. If there is no shroud, only the force vectors on the vanes need to be considered for the prediction of the performance of TVC. The fluid interferences induced by the vanes and the shroud violate the linear-proportional relation between the side force and the deflection angle of vanes in the linear range shown by jet vanes operating without the shroud. Thus, the performance prediction of vanes acting within the TVC shroud requires not only the investigation of the operation of jet vanes themselves, but also the characterization of the momentum interaction between vanes and the shroud.

The purpose of this paper is to investigate the side-force characteristics of vanes located in the TVC shroud with X formation through theoretical modeling, numerical study, and experiments.

II. Aerodynamic Characteristics of Jet Vanes

The number of vanes is usually four, and they are arranged in +- or X-formation (Fig. 2). In geometrical point of view, X formation is just a + formation rotated 45 deg. But if the alignment of the vanes are related with the aerodynamic surface or the position of umbilical cable of the missile body, the vane system with + arrangement moves two vanes to provide pitch or yaw force, whereas X arrangement vane system moves four vanes. The + formation is preferred as it produces a wider linear range of side forces to the deflection angle because only two vanes facing the same direction are deflected to provide the required control force. However, if the required side force cannot be sufficiently achieved with the + formation the X formation can be an alternative because all four vanes are deflected (Fig. 2). In terms of the linearity of vane performance and the convenient installation of vane actuators, vanes are placed at the end section of the nozzle. In typical cases the TVC shroud surrounds vanes to protect the control system of vanes from penetration of hot exhaust gas during the launch in a canister as this study concerns.

A. Semi-Empirical Model of Aerodynamic Force of Vanes and a Shroud

If no shroud is adopted and the vanes are placed at the end section of the nozzle, a linear theory or a simple semi-empirical model of shock waves can be employed to predict the aerodynamic force on vanes. However, if a shroud is used shock waves produced by vanes impinge on the shroud wall and so increase the pressure on the shroud wall (which was described in detail in the Section II.B.2). Modeling the force presents greater difficulty as the center of pressure and the direction of the force on a shroud vary according to the deflection angle of the vanes (Fig. 2). Thus, the magnitude and direction of the side force caused by the shroud depend on the angle of attack of not only the operating vane but also its neighbor vanes. Moreover, in case of vanes with X formations all four vanes operate so that the required control force is achieved and the relative position of each vane affects the additional force on the shroud wall. For this reason a new model that can predict the performance of vanes acting within a shroud is required. The basic ideas of a semi-empirical model in this study are based on following: 1) evaluation of parameters affecting the side force and thrust loss induced by jet vanes acting within a shroud and the modeling of the resultant force with the combination of the parameters; 2) modeling of the additional force caused by overpressure on the shroud wall, which is induced by the impingement of shock waves on the wall; and 3) transformation of the resultant force of vanes with an X formation arrangement to missile axis.

From experiments using cold-flow facilities, the parameters determining the side force can be listed as the deflection angle of vane,

the relative location of the vane in a nozzle, the relative vane size to the nozzle size, and so on.[14–16] Therefore, the side-force coefficient of the vane can be expressed as follows:

$$C_{\mathrm{Ls}} = \left(C_{s_1} + C_{s_2}\alpha\right)\left(l/r_e - C_{s_3}\right)\alpha(A_t/A_v) \tag{1}$$

C_{s1}, C_{s2}, C_{s3} are adjust coefficients. The adjust coefficient were obtained from the comparison between the polynomial equation (1) and the experimental data (Fig. 17), which are 0.0038, 0.000792, and 0.75, respectively in this study. Next, pressure increases on the shroud wall, induced by compression waves around the vane's windward side, must be modeled. The pressure increase on the shroud wall results in the reduction of side forces, while pressure decreases, induced by expansion waves around the vane's leeward side, cause an increase of the side force (see Fig. 2). Therefore, the side force of vanes in a shroud can be suggested as follows:

$$C_{\mathrm{Li}} = \xi_1\left[C_{L_s} + \xi_2\left(C_{L_{\mathrm{SEP}}} - C_{L_s}\right)\right]\xi_3\frac{\alpha}{\xi_4} \tag{2}$$

$$C_{L_{\mathrm{SEP}}} = \eta\frac{4\alpha\,\cos\,\alpha}{\sqrt{M^2-1}}$$

where η is 0.75 (Ref. 14). Other coefficients are listed in Table 1.

Because the vanes are arranged in an X formation, the yaw-force coefficient and the pitch-force coefficient considering the orientation of the vanes in an X formation are as follows:

$$C_{\mathrm{yaw}} = \kappa_1 C_{\mathrm{Lav}} \times \cos\,\alpha + \kappa_2 C_1 \tag{3}$$

$$C_{\mathrm{pitch}} = \kappa_3 C_{\mathrm{Lav}} \times \sin\,\alpha + \kappa_4 C_2 \tag{4}$$

where

$$C_1, C_2 = C_y \quad \text{or} \quad C_p \quad \text{(see Table 1)}$$

$$C_{\mathrm{Lav}} = 0.25\sum_{i=1-4} C_{\mathrm{Li}} \tag{5}$$

$$C_y = \left\{\sum_{i=1-4} C_{\mathrm{Li}} - 0.5(C_{L1} + C_{L2})\right\} \tag{6}$$

$$C_p = C_{\mathrm{yaw}} \times \tan\,\beta \tag{7}$$

κ_1, κ_2, κ_3, κ_4 of four vanes are defined in Table 1, and β were listed in Table 2. In Section III comparisons of the semi-empirical model with experiments are discussed in detail.

Table 1 Coefficients used in model

Head	Vane 1	Vane 2	Vane 3	Vane 4
ξ_1	0.77	0.7	1.0	1.0
ξ_2	−1	−1	1	1
ξ_3	2.037	2.037	2.037	2.037
ξ_4	22	18	60	50
η	0.75	0.75	0.75	0.75
κ_1	1	1	1	1
κ_2	−1	−1	1	1
κ_3	1	−1	1	−1
κ_4	1	−1	−1	1
C_1	C_y	C_y	C_p	C_p
C_2	C_p	C_p	C_y	C_y

Table 2 Force direction on the shroud to the deflection angle of vane

Deflection angle of vane, deg	β, deg
0	45
5	44
10	42
15	37
20	33
25	30

B. Numerical Analysis

A commercial software, FLUENT V.5.5 (Ref. 17), is used for numerical analysis. The numerical method applied for this study is based on a preconditioning scheme of the Navier–Stokes equation with unstructured finite volume discretization.[18] A coupled implicit k-ϵ turbulent flow model and a second-order upwind scheme were chosen. The boundary conditions applied for this study are described in detail in Section B.2.

1. Verification

To verify whether the numerical code, FLUENT V.5.5, is a suitable solver to analyze the aerodynamic characteristics of jet vanes and to find the numerical coefficient and numerical model suitable for this study, a model test was performed. A wind-tunnel test of a supersonic delta wing, which has a similar shape as a jet vane, was chosen for validation problem.[8] The aspect ratio of the supersonic wing was 0.5 with a square shape. Figure 3 shows a numerical domain and the features of a wing with surface grids. The Mach number of the freestream was 2.86, and every 10 deg of the angle of attack of the wing from 10 to 50 deg was simulated. The results indicate that the flow separation occurred at about 30 deg of the angle of attack at the leeward side of the wing, and flow separation was enlarged as the angle of attack increased. When flow separation occurred, an unsteady flow pattern induced by flow separation was observed. Table 3 and Fig. 4 show a comparison of the normal-force

Table 3 Comparison of normal-force coefficient

Angle of attack, deg	Experimental data	Numerical calculation
0	0	0
10	0.20	0.20
20	0.43	0.44
30	0.68	0.69
40	0.97	0.97
50	1.23	1.24

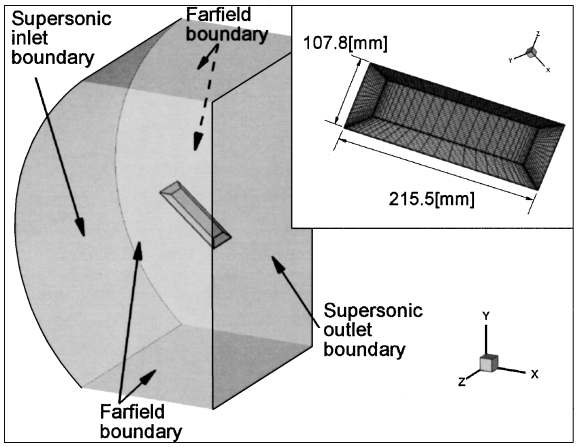

Fig. 3 Wing shape and grid system for a 40-deg angle of attack.

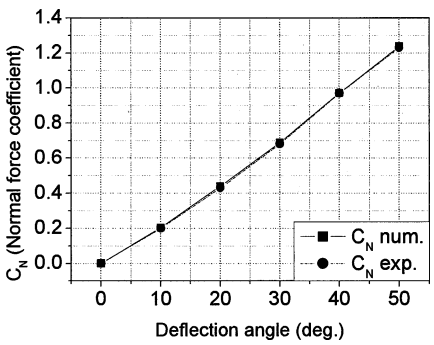

Fig. 4 Comparison of normal-force coefficient between numerical solution and experiment.

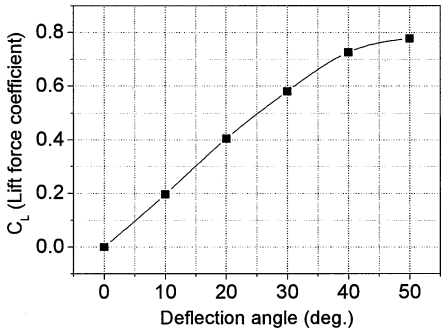

Fig. 5 Lift-force coefficient of single wing calculated by numerical solution.

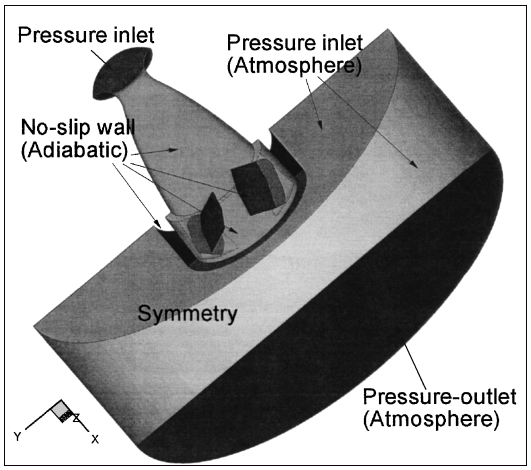

Fig. 6 Computational domain with applied boundary conditions.

coefficient C_N between the numerical results and experiments. Here, the normal-force coefficient was defined as

$$C_N = \frac{\text{Normal Force}}{q_\infty A_v} \tag{8}$$

Numerical results showed good agreement with the experiments. The comparison of unsteady solutions with steady solutions showed that the unsteady effect of flow separation on the magnitude of a normal-force coefficient was negligible. The lift coefficient of the wing linearly increased up to 30 deg of the angle of attack of the wing, and then the increase rate became slow at above 30 deg angle of attack of the wing (Fig. 5).

2. Numerical Analysis of Jet Vanes Within a Shroud

The jet-vane TVC system in this study is composed of four square-shape vanes to provide control force, vane bases to protect the vane shaft from hot combustion gas of the propellant, and a shroud surrounding the vanes to protect the actuator system from hot exhaust gas. The computational domain and the boundary conditions were described in Fig. 6. At the high-pressure inlet boundary the total pressure and total temperature were fixed with the condition of combustion chamber, whereas total pressure and total temperature were defined as 0.1013 MPa and 300 K for an atmospheric condition. At the outlet boundary all variables were extrapolated from the inner domain if outflow was supersonic, while pressure was fixed with atmospheric pressure and the other variables were extrapolated if the outflow was subsonic. The no-slip and adiabatic boundary conditions were applied for the wall boundary conditions. Figure 7 shows the detail geometry near the jet-vane units and a surface grid system in the case of a 20-deg deflection angle of vanes arranged in an X formation. The computational geometry of the jet-vane TVC system designed for the ground test was precisely modeled with a solid modeler, IDEAS,[19] and was recomposed to an unstructured tetrahedral grid system. Because of the X formation, only two vanes were

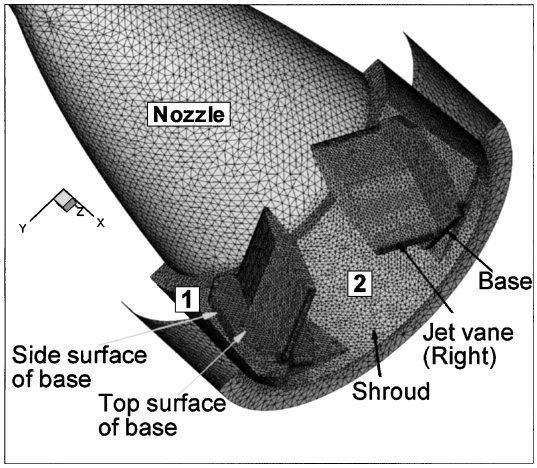

Fig. 7 Unstructured grid system for a 20-deg deflection angle of vanes.

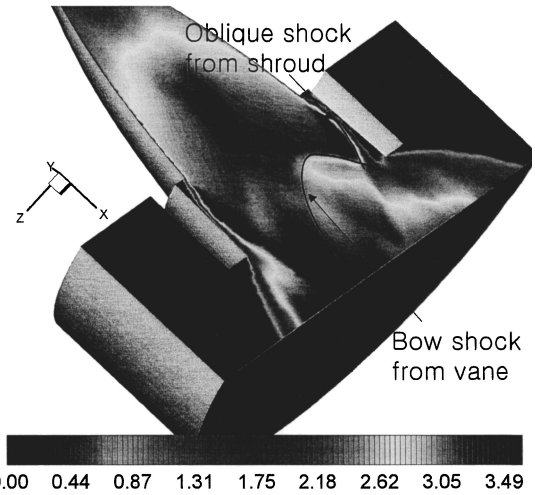

Fig. 8 Mach-number distribution on a symmetric plane for a 10-deg deflection angle of vanes.

included in a symmetric zone, which had the azimuth of 45 deg to the symmetric plane. The grid system was formed with about 0.41 million cells.

Numerical analysis was performed for six cases, which were 10, 20, and 25 deg of the angle of attack of vanes at both the high- and low-pressure conditions of the combustor. Figure 8 shows the general flow patterns in a jet-vane system. The flow patterns are as follows: Exhaust gas accelerating through a nozzle is suddenly expanded at the backward-facing step region where the nozzle and the shroud are connected. At the interspace between vanes, the accelerating supersonic flow is turned where it encounters the shroud wall, so an oblique shock wave occurs. On the other hand, at the region blocked by vanes the flow is compressed as a result of an oblique shock wave induced by the vanes. Because the vanes have blunt leading edges with a 2.5-mm radius to resist thermal ablation during motor operation, bow shock is formed and can affect a neighbor vane in special cases, as discussed in detail in Section II.B.2.c.

a) Side force induced by the TVC shroud. The shock wave impinging on the shroud wall causes the pressure of the shroud wall to increase so that additional side forces are generated. The resultant force induced by the shroud reduces the side force of the TVC system because the direction of the side force is opposite that of vanes, as shown in Fig. 2. The center of the resultant force on the shroud wall around the left vane (1 of Fig. 7) has a lower azimuth angle to the symmetric plane than that of the right vane (2 of Fig. 7). It, therefore, makes sense that the side forces caused by pressure increase on the shroud wall around the right and left vanes are not compensated

for each other. Moreover, the direction of the resultant side force is opposite that of the vane. Also, if the shock wave induced by the vane located at the opposite side of the left vane across its symmetric plane collides with the shock wave induced by the left vane, the side force of the jet-vane system deteriorates because the pressure on the shroud surface is drastically increased by the shock-shock intersection. Therefore the higher deflection angle of the vanes is, the more side force will be lost by the shroud. Figure 9 shows the facts just noted. The side force plotted here has an opposite sign to the side force by the vanes for convenience.

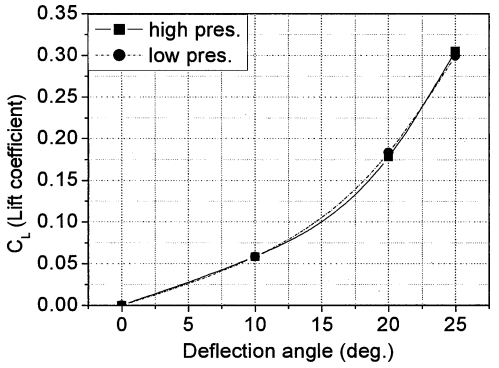

Fig. 9 Side force provided by the shroud (sign is opposite to real one, i.e., negative, in convenience).

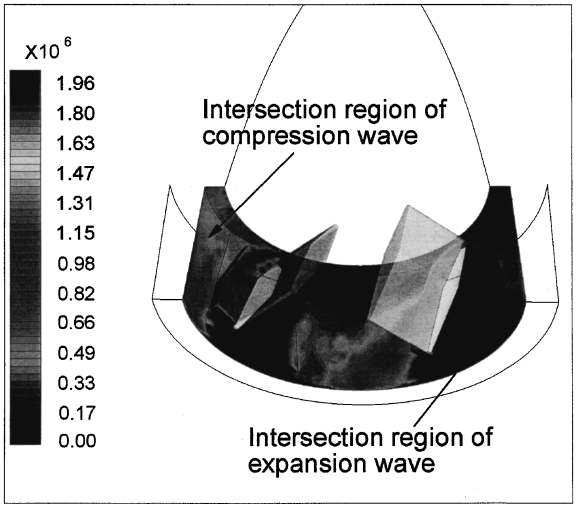

Fig. 10 Pressure distribution on the shroud surface at a 25-deg deflection angle of vane and high chamber pressure.

Figure 10 offers a typical explanation of the pressure distribution on the shroud wall, which is described so far.

b) Side force by vanes. Vanes are a major contributor of side force. The pressure difference between leeward and windward sides of a vane produces the side (lift) force. From the validation described in Section B.1, the side force increases linearly at a small deflection angle of the vane, but the increasing rate slows at a high angle of deflection of the vane. However, if the vanes are arranged in an X formation the relation of the force of the right vane to deflection angle of the vane might be different from that of the left vane. Because the intersection region of the compression wave exists between the left vanes as shown in Fig. 10, the shock wave produced by the opposite vane across the symmetric plane can impinge on the left vane. The possibility of the impingement depends on the relative vane size to the shroud size. If the shock impingement occurs, the side force of the vane might be abruptly increased. Figure 11 shows the pressure distribution on the surface of both the windward and leeward sides of the left vane according to the deflection angle of the vane. It was observed that the pressure at the rear-tip area of the windward side of the left vane was locally increased. This reflects the shock impingement onto the left vane at a high deflection angle. Also, such phenomena were observed from experiments as described in Section III.

c) Side force by the base of vane. The bow shock detached from the leading edge of the vane impinges on the base of the vane located at the root (see Fig. 7), which causes the pressure on the base surface to increase. The pressure increase on the base's top surface facing the gas flow (see Fig. 7) has little influence on the total side force because, as a result of the symmetric arrangement of the two vanes, the resultant force on the base's top surface is compensated with the resultant force of the neighboring vane's base. However, the side surfaces of the base produce side force like a vane. Figure 12 shows the effects. The absolute values of the side forces of both the right and left bases have opposite signs.

C. Experiments

A series of ground tests were performed by firing real-scale solid rocket motors in which four jet vanes are arranged in X formation as shown in Figs. 2 and 13. During the operation of rocket motors, each vane was individually deflected at typical angles assigned by remote controller. Figure 13 shows the rocket motor on the test stand with six-components balance to measure both thrust and side force and flame structure at a typical moment of vane deflection.

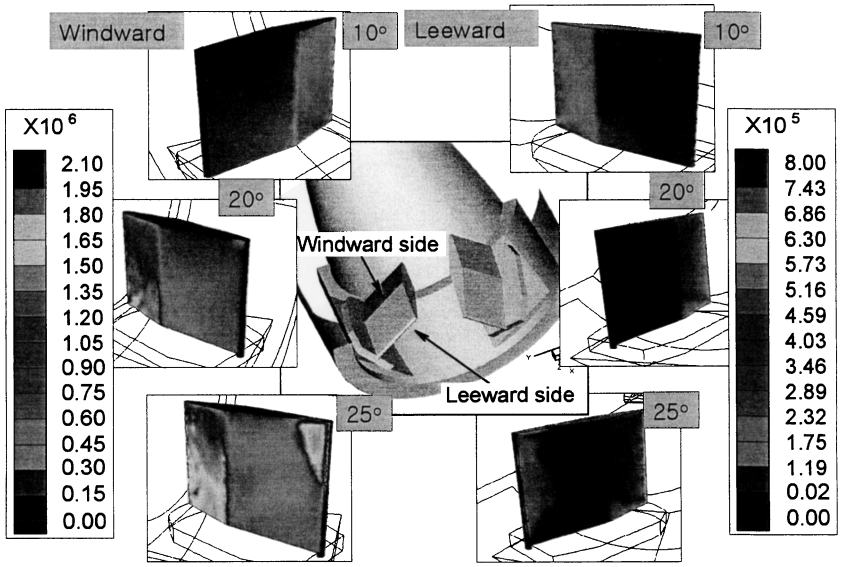

Fig. 11 Pressure distribution on the left vane surface.

The material of the vanes is carbon infiltration tungsten coated with ZrO_2 to protect thermal stress and to minimize ablation. The small round edge (2.5-mm radius) width of the vane is employed instead of the sharp edge to preserve the initial shape of the vane from thermal ablation induced by hot exhaust gas passing through a nozzle. The ablation of the vane was not severe, less than 1% of the cross section of vane (Fig. 13). More than eight tests were performed to establish an experimental database so as to characterize the side force of vanes. Some of them are addressed in Section III.

III. Discussion

Among many tests performed for this research, Fig. 14 represents a typical operation profile of four vanes, where the identification of the vane number is shown in Fig. 2. Each vane was simultaneously deflected at a certain angle, for example, 10, 15, 20, and 25 deg, and come back to the original position, zero deflection angle, from which the average side force of four vanes could be obtained at the deflection angle of vane. In the same way the side force of single vane could be obtained by moving each vane at a certain angle one by one. In this section the test data and the theoretical calculation based on the semi-experimental model addressed in Section II.A are compared and analyzed to characterize the vane's performance.

A. Thrust Loss

The thrust loss is caused by vanes blocking the exhaust gas inside the shroud. Figure 15 shows a comparison of the thrust–time history between the ground test and the prediction using the semi-empirical model described in Section II.A. Thrust is normalized by the maximum thrust if no vane is installed, whereas time was normalized with the total operation time of the motor. The thrust–time curves of the experiment and the prediction are very close to each other. Because the thrust loss cannot be directly measured by ground tests, it is indirectly obtained from the difference between the predicted total impulse without vanes and a total impulse of experiment with vane operation. About 6.1% thrust loss was predicted even though 6.8% thrust loss was estimated.

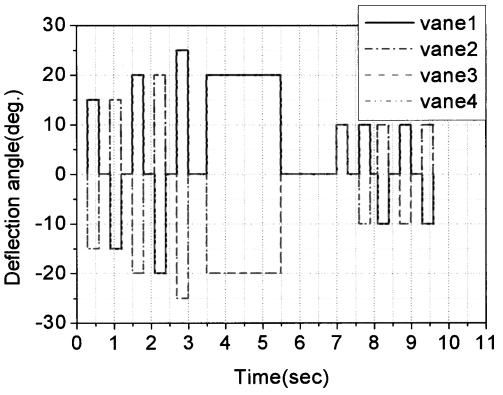

Fig. 14 Typical operation profile of four vanes.

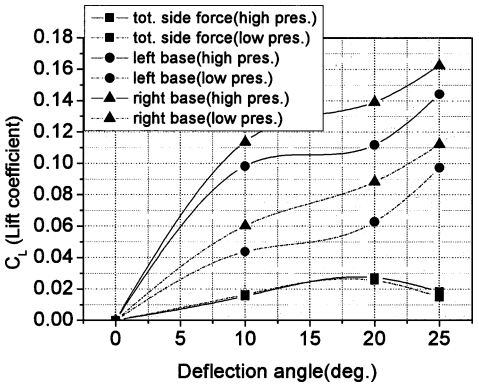

Fig. 12 Side-force (lift) coefficient provided by the base of vane.

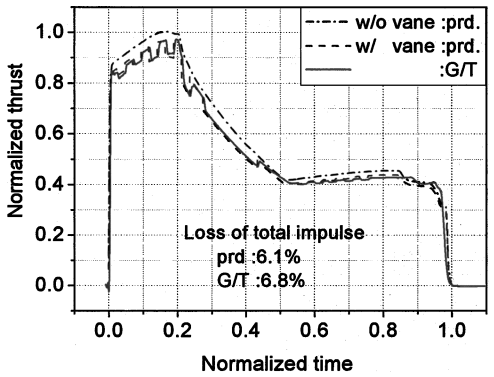

Fig. 15 Thrust vs time curve for vane's operation shown in Fig. 13.

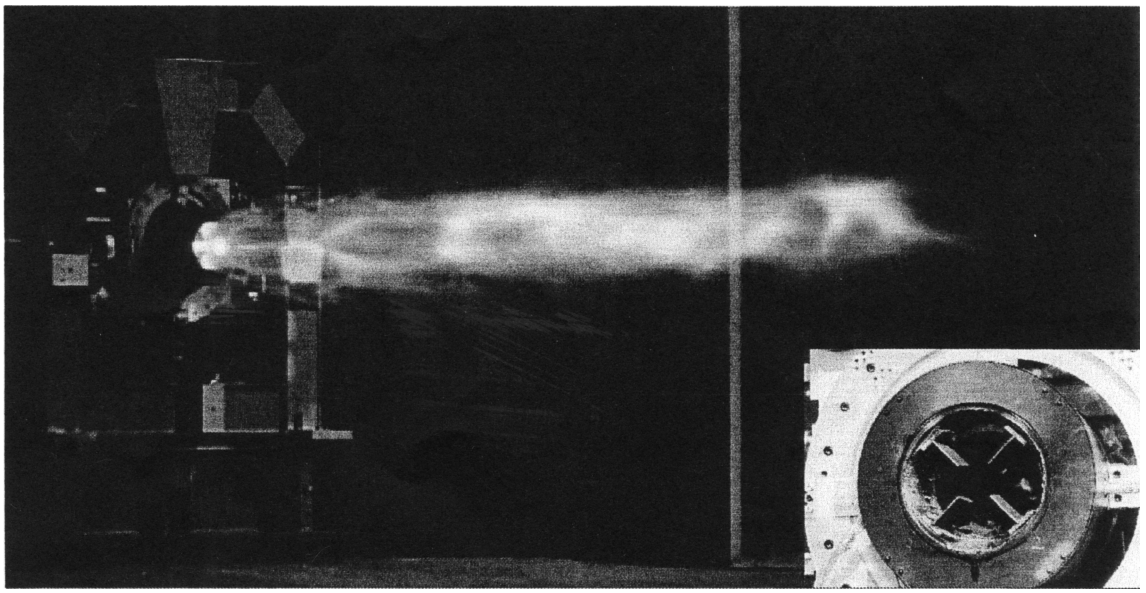

Fig. 13 Snapshots during firing test and after test (zoomed).

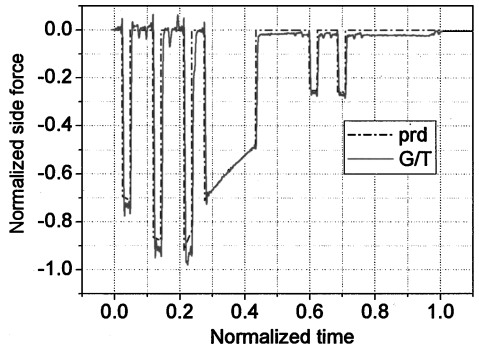

Fig. 16 Side force vs time curve for vane's operation shown in Fig. 13.

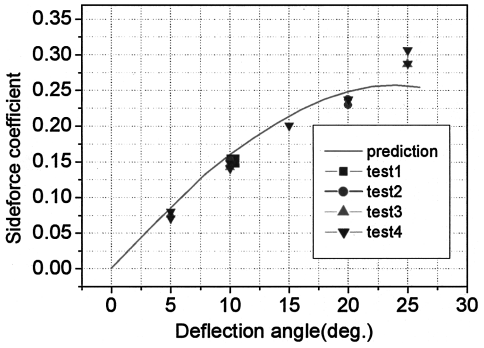

Fig. 17 Resultant side-force coefficient to vane's deflection angle.

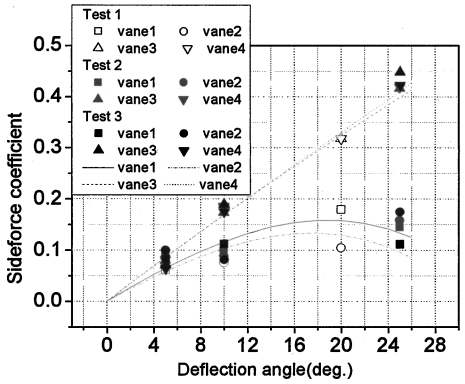

Fig. 18 Side-force coefficient of each vane to deflection angle.

B. Side Force

Figure 16 shows the side force vs time history in which prd means the prediction based on the semi-empirical model. The side force is normalized with a maximum side force predicted. At the deflection angle of the vane, 25 deg, the side force is predicted to be about 8% less than in the experimental result, while about 4% greater than experimental data at a 20-deg deflection angle of the vane. However, there are almost no differences between predictions and experiments at 10 and 5 deg (Figs. 16 and 17).

To analyze why the discrepancy is relatively large at a 25-deg deflection angle of the vane, the aerodynamic characteristics of each vane are inspected by deflection of vanes one by one. Figure 18 represents the side-force coefficients of each vane obtained by ground tests. The trends of the four vanes in terms of the side-force coefficients vs deflection angles of the vane are not same as each other. Side-force coefficients of vane nos. 1 and 2 are less than those of vane nos. 3 and 4. The reason is that the side force is reduced by the force produced on the shroud wall in the interaction region of the compression wave while it is increased in an interaction region of the expansion wave as shown in Section II.B.2.b and Fig. 10. This is the unique characteristic of jet vanes operating in X formation within a shroud. In addition, the side-force coefficient of vane no. 2 at 25-deg deflection angle is much larger than that at 20-deg deflection angle. Numerical analysis of the jet-vane TVC system provides physical insight in finding the reason for such a sudden increase in side forces at a 25-deg deflection angle as described in Section II.B.2.a. At a 25-deg deflection angle of the vane, the distance between the leading edges of the two vanes, nos. 1 and 2, at the intersection region of compression becomes narrow enough for shock waves provided by the vanes to intersect each other. If the shock wave produced by the vane across the symmetric plane impinges on the acting vane, the pressure on the vane surface, which the shock wave encounters, is abruptly increased, so that the side force is drastically increased. There is a critical distance at which these phenomena occur at around a 22-deg deflection angle of the vane in this study. This is the reason that the experimental result is larger than the prediction at a 25-deg deflection angle because the semi-empirical model described in Section II does not count on the impingement of shock starting from a neighbor vane.

IV. Conclusions

Jet vanes are being widely used as TVC units for advanced tactical missile systems because jet vanes produce both the required side force and roll moment, which allowed the advent of vertical-launched missiles. However, theoretical literature concerned with jet vanes are very limited, and particularly little published research is specifically related to jet-vane systems with the TVC shroud.

The semi-empirical model developed in this research was compared with experimental results, and some important physical phenomena were found by the integrated analysis of a semi-empirical model, numerical analysis, and experiments:

1) The side-force coefficient of four vanes surrounded by the TVC shroud departs from the linear relation to the deflection angle of the vane over 10 deg, and the increasing rate is decreased as a result of the negative side force induced by the shroud wall.

2) If four vanes are arranged in an X formation, the aerodynamic characteristics of fours vanes are not the same for each other and are very unique. Each vane must, therefore, be modeled in consideration of the fact that side-force coefficients of vanes placed in the interaction region of the expansion wave are linearly increased to the deflection angle of the vane, whereas the side-force coefficients of vanes in the interaction region of compression wave have a parabolic trend.

3) With deflection angles of vanes over 22 deg as in this study, the shock wave produced by the vane placed across the symmetric plane impinges on the vane located at the intersection region of compression region, resulting in an abrupt increase of side force of the vane.

References

[1]Danielson, A. O., and Dillinger, R. B., "Investigation of Thrust Vector Control for High-Alpha Pitchover," AGARD CP-451, 21-1, AGARD, March 1988.

[2]Sutton, G. P., *Rocket Propulsion Elements*, 6th ed., Wiley, New York, 1992, pp. 523–535.

[3]Loyd, R., and Thorp, G. P., "A Review of TVC Systems for Tactical Missiles," AIAA Paper 78-1071, July 1978.

[4]IMI Summerfield, *Thrust Vector Control*, Technical Brochure, Royal Ordnance, 1988.

[5]Hajime, O., *Reference Guide to World Missile Systems*, Shinkigensha, Tokyo, Japan, 2000.

[6]Facciano, A. B., and etc., "Evolved SeaSparrow Missile Jet Vane Control System Prototype Hardware Development," *Journal of Spacecraft and Rockets*, Vol. 39, No. 4, 2002.

[7]Ascher, H. Shapiro, *The Dynamics and Thermodynamics of Compressible Fluid Flow*, 1st ed., Vol. 2, Wiley, New York, 1954, pp. 703–744.

[8]Robert L. S., Jr., and Milton, L., "Wing-Alone Aerodynamic Characteristics for High Angles of Attack at Supersonic Speeds," NASA-TP-1889, July 1981.

[9]Webster, W. P., and Shang, J. S., "Thin-Layer Full Navier–Stokes Simulations over a Supersonic Delta Wing," *AIAA Journal*, Vol. 29, No. 9, 1991, pp. 1363–1369.

[10]Ripley-Lotee, M. J., and O'Neil, S. M., "Jet Vane Thrust Vector Control—A Neglected Technology with New Horizons," Chemical Propulsion Information Agency, CPIA 308, Vol. 3, Dec. 1979.

[11]Roger, R. P., Chan, S. C., and Hunley, J. D., "CFD Analysis for the Lift and Drag on a Fin/Mount Used as a Jetvane TVC for Boost Control," AIAA Paper 95-0083, Jan. 1995.

[12]Oh, Y. H., *CFD Studies of Jet Vane Control Actuation System*, Presentation Material of Hughes Aircraft, Hughes Aircraft, Seoul, Korea, May 1997.

[13]Danielson, A., "Inverse Heat Transfer Studies and the Effects of Propellant Aluminum on TVC Jet Vane Heating and Erosion," AIAA Paper 90-1860, July 1990.

[14]Ayre, V. H., "Analysis and Experiments on Jet Vane Thrust Vector Control," U.S. Army Missile Command, TR RG-73-4, Alabama, Feb. 1973.

[15]Zhiheng, L., "Aerodynamic Design Research of the Gas Vane of a Solid Motor," National Air Intelligence Centre, NAIC-ID(RS)T-0272-96, China, July 1996.

[16]Clien, Z., "Analytical Investigation on the Behavior of Jet Vane," Technical Conference on Thrust Vector Control, TR ASB-93-1202, Taejon, Korea, Dec. 1993.

[17]FLUENT, Inc., *Fluent v. 5 User's Guide*, Vol. 1–4, Dec. 2001.

[18]Weiss, J. M., and Smith, W. A., "Preconditioning Applied to Variable and Constant Density Time-Accurate Flows on Unstructured Meshes," AIAA Paper 94-2209, June 1994.

[19]*I-DEAS ms.9.0 User's Guide*, Electronic Data Systems, 2002.